Engineering Transactions, **71**(4): 571–593, 2023, doi: 10.24423/EngTrans.3157.20231123
Institute of Fundamental Technological Research Polish Academy of Sciences (IPPT PAN)
Université de Lorraine • Poznan University of Technology

Research Paper

The Effect of Ni-TiO_2 and Ni-TiO_2-graphene Coatings and Heat Treatment Hardening on Solid Particles Erosion Resistance of Grade 410 Stainless Steel

Wissam KHALID, Hamza A. AL-TAMEEMI*

Mechanical Engineering Department, University of Baghdad
Al Jadriya, Baghdad, 10070, Iraq; e-mail: W.AlBawe1803M@coeng.uobaghdad.edu.iq

*Corresponding Author e-mail: hamza.al-tameemi@coeng.uobaghdad.edu.iq

Erosion by solid particles is a serious problem in many applications, especially in rotary machines with steel blades. Many coatings are currently being developed to improve erosion resistance. This study focuses on investigating the solid particles erosion (SPE) resistance of AISI 410 stainless steel and improving the SPE resistance using three different anti-wear techniques: hard coating (Ni-TiO_2), hard coating with low shear resistance (Ni-TiO_2-graphene) and hardening by heat treatment. The study also investigates the effect of different factors, including impact angle, jet pressure (particle speed) and solid particle type on each of the four types of specimens.

The investigated anti-wear techniques improved the erosion wear rate by different percentages, such as 35.2% using Ni-TiO_2 coating, 36% using Ni-TiO_2-graphene, and 53.75% using heat-treatment when silica sand, a 45° impact angle and a speed of 36.72 m/s were used. The results indicate a ductile erosion mechanism as the weight loss decreases with an increase in the impact angle. The investigated coatings were found to provide more stable erosion resistance under different impact angles. Surface roughness was reduced after SPE for coated surfaces, and surfaces showing a lower wear rate may not necessarily show less change in surface roughness. It was observed that deformation in the form of waviness only occurs when the surface is impacted by small rounded particles at a 45° angle. Wear rate parameters were calculated, which can be used to estimate the wear rate for the investigated material under various conditions.

Keywords: solid particles erosion; wear rate; wear resistance; erosion testers; AISI 410 stainless steel; Ni-TiO_2 coating; Ni-TiO_2-graphene coating.

1. Introduction

In many applications, high-speed rotary machines exposed to solid particles (sand and dust) suffer from erosion. Many of these machines use steel blades that

can be affected by erosion, leading to modification in their airfoils and a decrease in their performance [1]. Erosion in the vanes and rotor blades of the gas turbine compressor can be reduced by using different coatings, as shown by previous studies [1, 2]. Additionally, another study showed that certain thermal sprayed coatings can reduce slurry erosion caused by silt sediments in flowing water, which may cause failure of the steel used in hydro-power turbine components [3]. Accordingly, research in the field of surface deterioration due to the impact of particulate matter is expanding to tackle this type of surface failure. When a surface loses particles (chips) due to repetitive impacts by relatively small solid particles carried by a fluid current, this weight and volume loss is called erosion wear or Solid Particles Erosion (SPE). The cumulative removal of material from the surface occurs by cutting or fracturing, where the kinetic energy of the solid particles is dissipated through many mechanisms, such as plastic deformation, crack initiation and propagation, friction, and heating. Many factors affect these mechanisms, including particle's velocity, impacting angle, density, shape, and hardness, as well as those of the eroded surface [4].

The two main types of SPE mechanisms are ductile and brittle but transition between these two is also possible. When the surface material is removed by plowing or cutting, which are also known as plastic flow, ductile SPE occurs with the highest wear rate at impingement angles between 20° and 30°. If the material removal occurs due to crack propagation and intersection, brittle SPE will be the dominant mechanism and the greatest wear rate takes place at a high incident angle. which is around 90° [4]. Based on the cutting mechanism, Finnie [5] proposed a first model to predict the amount of material loss due to SPE. In this model, the volume removed from the surface by the solid particles can be determined by the path taken by the particles during penetration into the surface and as they roll over it, according to the forces at the particle's tip [5]. At low angles of incident, the cutting mechanism is assumed to be the dominant in ductile SPE [6]. At high impingement angles, the ductile SPE is assumed to be caused by other mechanisms, such as embrittlement due to work hardening [7], high localized temperature due to impact, and fatigue due to repeated plastic deformation [8].

There are numerous forms of surface modification techniques used to combat wear. The most widely employed methods of surface modification to improve SPE are coatings, heat treatment, surface treatment by diffusion and surface treatment by mechanical processing. Surface coating is conducted using physical or chemical methods to form a protective layer on the surface, which can be hard or soft.

Using materials with high fracture toughness or high hardness to improve SPE resistance by preventing crack propagation and dissipating the particle's kinetic energy through fragmentation are the techniques used in coatings. Among

these, TiN-based coatings have been the most widely employed industrial SPE resistant-coatings in aircraft engines until recently. As a result, numerous investigations on monolithic and multilayer TiN-based systems have been conducted. Immarigeon *et al.* [1] demonstrated that TiN single-layer coatings created using different deposition processes exhibit significant variations. According to Hassani *et al.* [9], the considerable variation in coating thicknesses may have had a significant impact on the results. Other titanium nitride-based coatings such as TiSiN nano-composite coatings have been studied. Azzi *et al.* [10] and Zeng *et al.* [11] demonstrated that TiSiN nano-composite coatings are more wear resistant than TiN and other nitride coatings, while Wei *et al.* [12], Azzi *et al.* [10], and Bousser *et al.* [13] demonstrated that TiSiCN coatings are also highly wear resistant when compared to TiN, TiSiN, CrN. Furthermore, Boussers *et al.* [14] showed that CrSiN coatings outperformed CrN coatings. In general, for these coatings, when a nano-composite structure was formed, minimal erosion rates were identified. Shao *et al.* [15] investigated the mechanical and anti-corrosion properties of an electroplated nickel nanocomposite containing a relatively small percentage of TiO_2. It was found that nanocomposite coating is smoother and it has more compact surface than pure Ni coatings. It was also found that the hardness was higher and wear rate was reduced. The results of this study show that including TiO_2 into nanocomposite Ni-based coatings can be advantageous for improving wear and corrosion resistance. Even for coatings formed with thermal spray, specifically High Velocity Flame Spray (HVFS), adding TiO_2 alone or TiO_2-Al_2O_3 to the Ni-based coating demonstrated to reduce erosion wear [3]. In another study [16], adding TiO_2 and graphene oxide to form Ni-W-TiO_2-graphene oxide coating using ultrasonic-assisted pulse electrodeposition was studied. The results showed a significant improvement in wear resistance of such a coating compared to the Ni-W coating. Since a sliding wear test was conducted, the graphene oxide acted as self-lubricant, further reducing the wear rate.

The reviewed studies show the importance of studying the problem of surface erosion caused by solid particles. Although preventing surfaces from exposure to harder particles moving at high speed may be unavoidable, protecting the surface by applying different techniques such as coating and hardening emerges as a possible solution. Many studies investigated the effect of different surface protection methods applied to different substrates. However, to the best of authors' knowledge, no available studies considered studying the SPE resistance for AISI 410 stainless steel, which can be used for aerospace, marine and industrial gas turbine engines [2], coated with hard coating of Ni-TiO_2 or hard coating with low shear resistance of Ni-TiO_2-graphene, and subsequently comparing the results with the uncoated substrate and heat treated substrate. Accordingly, the current study aims to address this research gap.

2. Materials and experiments

2.1. Substrate

Stainless steel grade 410, according to ASTM A 240, is one of the most widely used materials due to the suitability of its properties for a wide range of applications, offering corrosion resistance and moderate price. In recent years, the use of chromium ferritic stainless steel has grown significantly across various technological domains, including chemical industries and oil and gas transportation. Because of its robust corrosion resistance and superior mechanical qualities, it is an excellent choice for a variety of applications [17]. Table 1 and Table 2 show the mechanical properties and chemical composition for the stainless steel grade 410 used in this study, respectively. The stainless steel grade 410 used in the current study is employed as a reflector; therefore, it has a smooth surface with a relatively low roughness of 0.254 μm. Consequently, no mechanical grinding or polishing was needed. However, degreasing was conducted ultrasonically in ethanol.

Table 1. Mechanical properties of stainless steel grade 410.

Yield strength [MPa]	290
Ultimate tensile strength [MPa]	444
Modulus of elasticity [GPa]	200
Density [g/cm^3]	7.73
Vickers hardness HV	148
Reduction percentage of area	65

Table 2. Chemical composition of stainless steel grade 410.

Element	Amount [%]	Element	Amount [%]
Ti	0.0073	C	0.0047
V	0.0609	Si	0.578
W	less than 0.005	Mn	0.269
Pb	less than 0.001	P	Less than 0.0005
Sn	0.0057	S	Less than 0.0005
B	less than 0.001	Cr	12.1
Ca	0.0009	Mo	0.0332
N	less than 0.01	Ni	0.103
Se	less than 0.002	Al	Less than 0.001
Sb	less than 0.003	Co	0.0037
Ta	less than 0.01	Cu	0.0569
Fe	86.6	Nb	0.0306

2.2. Coating

The stainless steel samples were coated using an electroplating process to achieve metal matrix composites (MMCs). Electroplating is a generic term for methods that result in a metal coating on a solid substrate by direct electric current. The cathode (negative electrode) of an electrolytic cell is the part to be coated, while, it is common for the anode (positive electrode) to be a block inert conductive material that is used as the electrolyte. An external power supply provides the current. In this study, the anode is a nickel plate, and the cathode is the steel specimen. Table 3 shows the chemicals used for the electrolyte bath along with other coating parameters. For the first group of specimens, 10 g of nano TiO_2 (30 nm) were used to produce the Ni-TiO_2 [18]. For the second group of specimens, 5 g of nano TiO_2 (30 nm) and 5 g of graphene were used to produce the TiO_2-Ni-graphene coating [19]. A digital display microhardness tester with a pyramid-shaped indenter was employed for the hardness measurement in which a load of 100 g was applied for 10 seconds. Accordingly, the hardness was found to be 148 HV for the stainless steel, 177 HV for the stainless steel coated with Ni-TiO_2, and 166 HV for the stainless steel coated with Ni-TiO_2-graphene.

Table 3. Chemicals and conditions for electroplating.

$NiSO_4$ $6H_2O$ (nickel sulfate)	300 g/L
$NiCl_2$ $6H_2O$ (nickel chloride)	50 g/L
H_3BO_3 (boric acid)	40 g/L
TiO_2	5 or 10 g/L
Graphene	5 or 0 g/L
SDS (sodium dodecyl sulfate)	0.2 g/L
Temperature	50°C
Current density	4 A/dm^2
Magnetic stirring	300 rpm
Coating duration	10 min
TiO_2 particles size	30 nm
Graphene thickness	6–8 nm
Graphene average particle diameter	15 μm

The average thickness of the (Ni-TiO_2) coating was about 14.3 μm, while the average thickness of the Ni-TiO_2-graphene coating was about 19.5 μm, as shown in Fig. 1. These measurements were performed using the field emission scanning electron microscope (FESEM). According to the supplier of the chemical materials used in this study, the average uniform size of the TiO_2 particle is 30 nm, while the graphene has a platelet morphology with a thickness of 6–8 nm and an

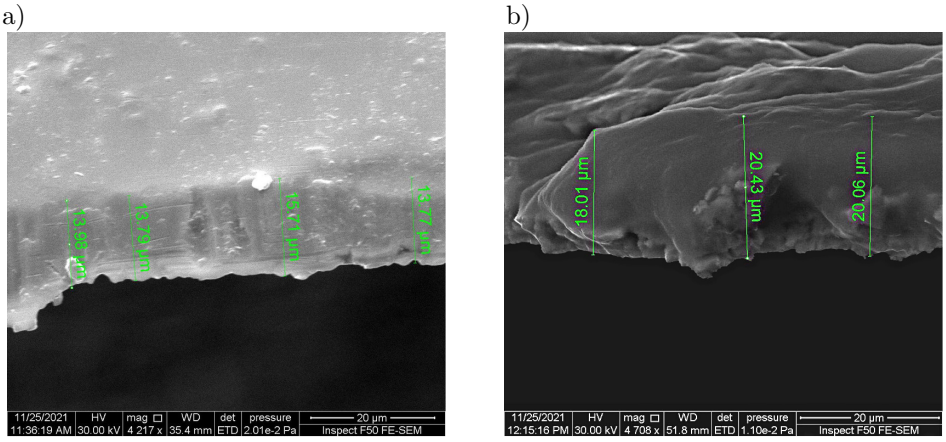

FIG. 1. FESEM images showing the coating thickness:
a) TiO_2-Ni coating area, b) TiO_2-Ni-graphene coating.

average particle diameter of 15 microns. This considerable difference in morphology between TiO_2 and graphene shows that the precipitation of Ni molecules and nano TiO_2 on the steel substrate is expected to form a more consistent and smoother coating than the graphene-containing coating, due to the non-uniform shape and size of graphene particles. One of the possible scenarios for the coating formation starts with the physical bonding (Van der Waals force) between the negatively charged graphene and the positively charged TiO_2, which makes an even more non-uniform morphology, and then followed by precipitation with the Ni molecules on the anode steel substrate [20].

2.3. Heat treatment process

As one of the anti-erosion techniques investigated in this study, improving the hardness of the stainless steel 410 by heat treatment was conducted. According to [21], this stainless steel can be hardened by heating in an atmospheric furnace to 982°C and then cooled by air until reaching room temperature. Next, it is followed by tempering for four hours at 204°C. This process results in forming a martensite structure with precipitated carbide. Using this process, it was possible to increase the hardness from 148 to 200 HV.

2.4. Solid particles

Three types of solid particles were used in this study. Figure 2 shows the first type of solid particles used (SP1) consisting of micro glass beads that are mostly spherical with an average particle size of 99 µm. The chemical compositions for this sand are shown in Table 4 and were measured using EDX analysis.

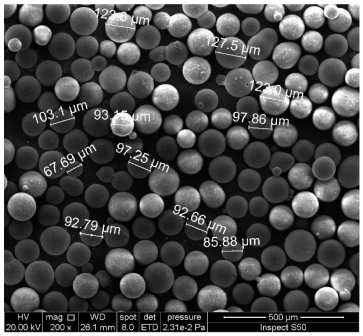

FIG. 2. SEM images at different magnifications for the micro glass beads (SP1).

Table 4. Chemical composition of the solid particles used.

Chemical composition [%]	SP1	SP2	SP3
SiO_2	71.69	71.58	96.29
CaO	15.30	13.92	–
Na_2O	7.29	13.11	–
MgO	5.66	–	–
Al_2O_3	–	1.39	3.714

Figure 3 shows the second type used of solid particles (SP2) which consists of glass beads. As shown in Table 4, there is a slight difference between the chemical composition of this type and the first type SP1. It can be noticed that the main difference is in the percentage of Al_2O_3. These particles are predominantly spheres, similar to the first type, with an average particle size of 310 µm. The hardness is obtained from the literature and it is 5.5 Mohs' hardness [22].

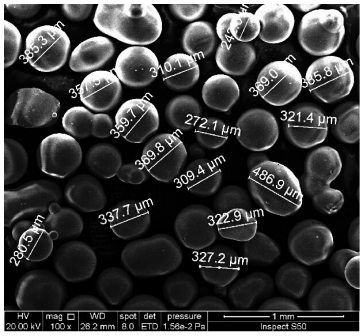

FIG. 3. SEM images of the glass beads (SP2) at different magnifications.

Figure 4 shows the third type of solid particles (SP3) used, which is silica sand. Table 4 shows the prevalence of SiO_2 in this type of solid particles com-

pared to the first two types. These particles do not have a rounded shape as the first two types. Figure 4 clearly shows the sharp edges of this sand. Although the deviation in the size of these particles is much higher than that of the other two types, the average particle size is found to be 330 μm. The hardness is obtained from the literature and falls in the range of 6–7 Mohs' hardness [22].

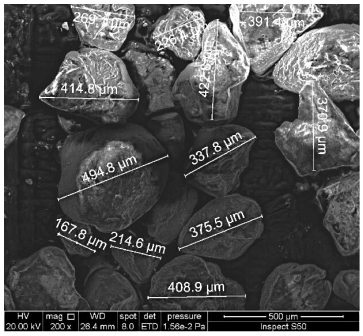

FIG. 4. SEM images of silica sand (SP3) at different magnifications.

2.5. Apparatus

The gas jet erosion testing machine used in this study was manufactured according to ASTM G 76 [23] and it includes an air compressor, air tank, sandblasting chamber, specimen holder, mixing nozzle, and a pressure adjusting valve. To measure the speed of particles, a high-speed camera was used. Figure 5 illustrates the nozzle and specimen configurations as well as the working distance. The nozzle's orifice diameter is 5 mm, and the working distance is fixed at 15 mm. The apparatus operates based on the principle of dragging solid parti-

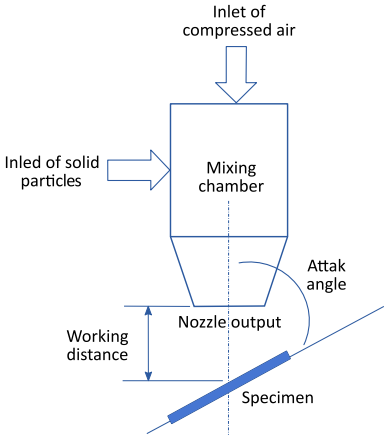

FIG. 5. Schematic illustration of the erosion testing apparatus.

cles into a stream of compressed air in order to be applied to the tested specimen using a jet nozzle. The testing apparatus is designed to apply a stream of solid particles on the tested specimen to erode the surface as the particles move at a controlled velocity and the specimen can be aligned at different angles. The results of the test include the difference in the specimen's weight before and after the test, as well as the difference in surface roughness before and after the test.

3. Design of experiments

Four groups of 410 stainless steel specimens are tested, each hardened by thermal treatment, coated with Ni-TiO_2, coated with Ni-TiO_2-graphene, and uncoated 410 stainless steel without coating or heat treatment. Each specimen is 1.5×1.5 cm. Also, in order to predict the effect of the erosion particle's impact angle, three types of supports are considered: (i) when the sample faces the jet directly vertically, i.e., the angle is 90° between the sample and the jet, (ii) when the sample faces the jet with an angle of 45°, and (iii) when the sample faces the jet with an angle of 60°. Three different values of pressure are used to examine the influence of varying jet pressure, and consequently varying particle's speed on erosion wear rate. Three different types of solid particles (SP) are used in this study: (i) micro glass beads (spherical shape with an average size of 99 μm), (ii) glass beads (spherical shape with an average size of 310 μm), and (iii) silica sand (irregular sharp edges with an average size of 330 μm). The test time was fixed, set at 10 minutes for all tests. The distance between the nozzle outlet and the specimens was maintained constant at 1.5 cm.

Table 5 shows parameters setting for each test according to the full factorial arrangement. Considering the working conditions in Table 5, the total number

Table 5. Testing conditions and arrangement.

Sample	Sample material	Abrasive material	Impact angle (applied for each SP) [°]	Pressure (applied for each SP and each impact angle) [bar]
1	Stainless steel	SP 1 SP 2 SP 3	90 60 45	1 1.5 2
2	Coated with $TiO_2 + Ni$	SP 1 SP 2 SP 3	90 60 45	1 1.5 2
3	Coated with $TiO_2 + Ni +$ graphene	SP 1 SP 2 SP 3	90 60 45	1 1.5 2
4	Only heat treatment	SP 1 SP 2 SP 3	90 60 45	1 1.5 2

of tests was 216, with two replications for each of the 108 tests. The replicated tests showed consistency where the variation from the average values did not exceed 13% for very few tests and were under 7% for most of the tests. It is expected for the replicated tests to show some result disparity due to the uncontrolled parameters that may affect the results, such as the variation of the size and shape of the impacting solid particles as well as variations in the impacting speed and angle at the particle level.

4. Wear rate form used in this study

The wear rate formula used in this study is given in Eq. (4.1), where E may be expressed as a dimensionless value or expressed in mg/kg, as adopted in the current study

$$E = \frac{\text{eliminated mass of material}}{\text{erosive particle mass hitting surface}}. \tag{4.1}$$

This erosive wear rate is related to the properties of the eroded surface and the erodent as well as the testing parameters, as shown in Eq. (4.2):

$$E = \frac{K\rho U^2}{2H}. \tag{4.2}$$

The wear coefficient K is a dimensionless value that indicates the intensity of wear, ρ is the density of the eroded material, U is the velocity of the erodent particles, and H is the hardness of the eroded material [6]. It has been identified in previous studies [6, 24] that E is not always a function of U^2 and the general form of Eq. (4.2) can be written in the form of Eq. (4.3), where B is the coefficient that varies according to the characteristics of the target material and erodent, and n is the velocity exponent depending on the impact angle [24]

$$E = BU^n. \tag{4.3}$$

The coefficient B in Eq. (4.3) can be divided into two parameters to consider the effect of the solid particles and the target surface on the wear rate separately, as shown in Eq. (4.4). In this equation, A is the abrasivity of the solid particles, empirically defined as the ratio between the weight loss caused by any erodent to that caused by SP3 since it causes the highest weight loss. C is related to the wear coefficient K and other material parameters, as shown in Eq. (4.5):

$$E = AC^{-1}U^n, \tag{4.4}$$

$$K = \frac{2AH}{C\rho}. \tag{4.5}$$

5. Experimental results

5.1. Average weight loss

Figure 6 shows the average weight loss for all four types of specimens using different solid particles at different particle speeds and impact angles. This figure shows that the heat-treated stainless steel samples yield the best results as they show the lowest average weight loss compared to all other types of specimens under all operational conditions investigated in this study, including different solid particles, impact angles and impact speeds.

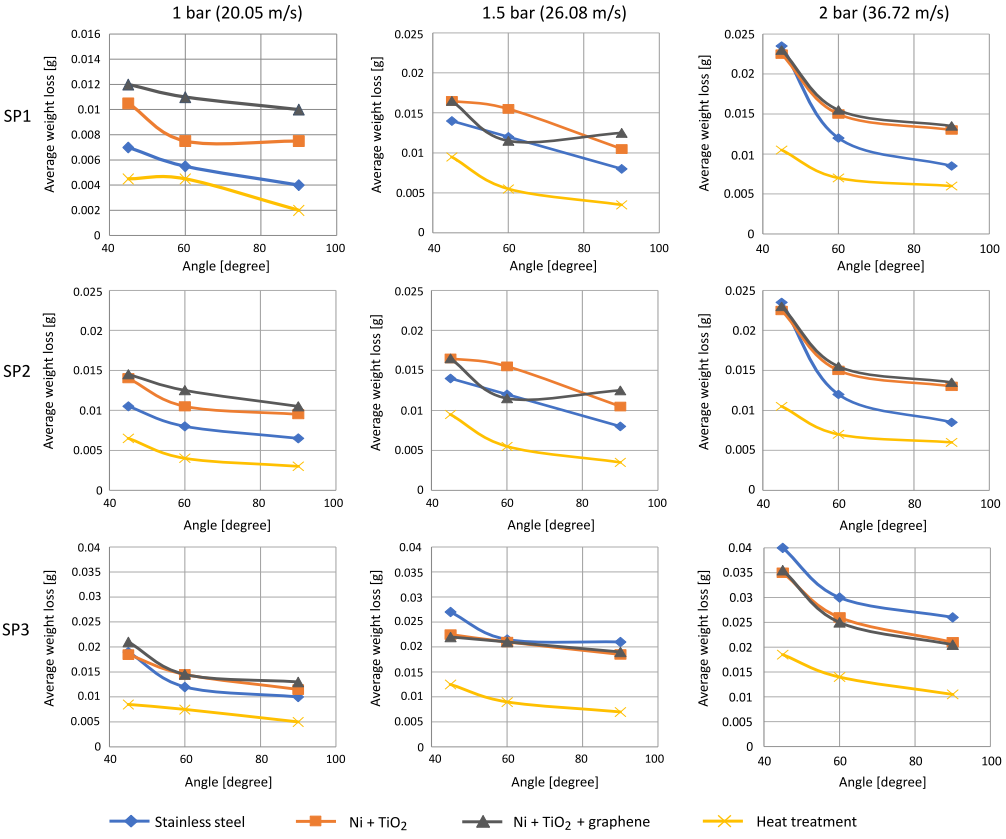

Fig. 6. Weight loss at different SP, impact angles and impact speed.

Also, erosion tests conducted with micro glass beads revealed that Ni-TiO$_2$ and Ni-TiO$_2$-graphene coatings do not provide effective protection against this type of erosion. However, analysis' details of calculating the weight loss distribution between the coating layer and the steel substrate indicate that less wear

occurs in the substrate of the coated specimens, implying that the coating layer may act as a sacrificial surface. In the current study, the mass removed from the coating and that removed from the substrate were calculated by finding the mass of the coating covering the tested area, using the coating density and coating volume, which can be calculated using the measurement of the coating thickness. Partial removal of the coating occurs when the weight loss measured after the erosion test is less than the weight of the coating covering the tested area. Otherwise, the weight loss after the test represents the sum of the coating weight covering the tested area and the weight loss from the steel substrate.

The data shows that in Ni-TiO_2 coating tests total removal of the coating occurred in 40.7% of cases and that for the Ni-TiO_2-graphene coating in 37%. In these tests, the average share for the substrate weight loss is 26.2% for Ni-TiO_2 coating and 30.3% for Ni-TiO_2-graphene coating. These percentages show that these coatings contribute significantly to reducing the wear of the substrate. It is observed that total coating removal occurs at the highest jet pressure when SP2 or SP3 is used.

The effect of changing the impact angle is evident, as the minimum weight loss is acquired at the right angle (90°) and for all conditions. This reveals that the erosion mechanism occurring on all types of surfaces is a ductile erosion. It can also be noticed that there is no significant difference in results between 1 bar and 1.5 bar pressure; while the difference is noticeable at 2 bar pressure. A similar trend is observed in the variation of weight loss with impact speed and angle when SP1 (the smallest round particles) and SP2 (the largest round particles) are used; however, weight loss is considerably higher when SP2 is used. Additionally, almost the same weight loss can be observed for Ni-TiO_2 and Ni-TiO_2-graphene coatings under specific conditions such as SP3, all pressures, all angles and SP2, all pressures, 45° and 90° angles.

Among the three solid particles investigated, SP3, which is almost the same size as SP2 but with sharp edges and a higher content of SiO_2, causes the highest weight loss. One the other hand, SP1, which is almost similar to SP2 in chemical compositions and geometry but smaller in size, leads to the least weight loss across all the investigated jet pressures and impingement angles, and for all types of specimens.

Although weight loss increases with increasing jet pressure due to the increase in particle velocity and consequently kinetic energy that increases the cutting and deformation depth, the sequence of the weight loss among the four types of specimens changes with increasing pressure. When SP3 is used, it can be seen that at high pressure, Ni-TiO_2-graphene specimens no longer show the highest weight loss among the other types of specimens. Instead, this coating shows higher erosion wear resistance compared to bare steel and Ni-TiO_2 coated steel. This improvement in the wear resistance of the Ni-TiO_2-graphene coating

under the impact of the sharp particles from SP3 lends support to the hypothesis assumed in this study for the effectiveness of adding more sliding characteristics into the coating in order to increase the gliding over the cutting behavior of solid particles on the impacted surface.

Under all the operational conditions investigated in this study, including different solid particles, impact angles and impact speeds, the heat-treated stainless steel samples show the lowest average weight loss compared to all other types of specimens. However, if the surface roughness after the SPE is considered, heat-treated stainless steel samples may not be the best, as it will be discussed in Subsec. 5.2.

5.2. Arithmetic roughness

5.2.1. Arithmetic roughness (Ra) in the jet direction. The roughness measurements for the samples before the erosion tests were 0.254 μm for the stainless steel, 0.645 μm for the specimens coated with Ni-TiO_2, 2.598 μm for the specimens coated with Ni-TiO_2-graphene, and 0.343 μm for the heat-treated specimens. Figure 7 shows the roughness measurements after the SPE tests conducted under different conditions. The first observation is the smoothening of the Ni-TiO_2-graphene-coated specimens and the roughening of the uncoated specimens under all the investigated conditions after the SPE tests.

It can be seen that smoothening occurs at higher impact angles under all pressures, while higher roughness occurs at lower impact angle, which may indicate greater deformation due to higher tangential force. It can also be seen that higher jet pressure (higher impact velocity) results in roughness. Increased roughness with decreased impact angle or increased jet pressure can be an indication of greater weight loss. These results are in line with the weight loss measurements in Fig. 6. In general, all the investigated anti-wear techniques result in lower surface roughness after the SPE tests compared to untreated stainless steel, since the stainless steel specimens always show the highest roughness. Figure 7 demonstrates that Ni-TiO_2 coating results in the lowest surface roughness after the SPE tests, almost under all the considered conditions, outperforming other types of specimens.

For SP2, the general trend in roughness with increasing impact angle is similar to that of SP1. It is very clear that SP3 increases roughness significantly more than when SP1 and SP2 are used, and this difference is more pronounced when higher jet pressure is applied. The sharp particles of SP3 are expected to induce higher roughness as well as weight loss. For SP3, it can be seen that the heat-treated specimens exhibit the lowest surface roughness after the SPE tests at the investigated pressures when compared to other types of specimens. The Ni-TO_2-graphene is the second best in terms of low roughness with values very

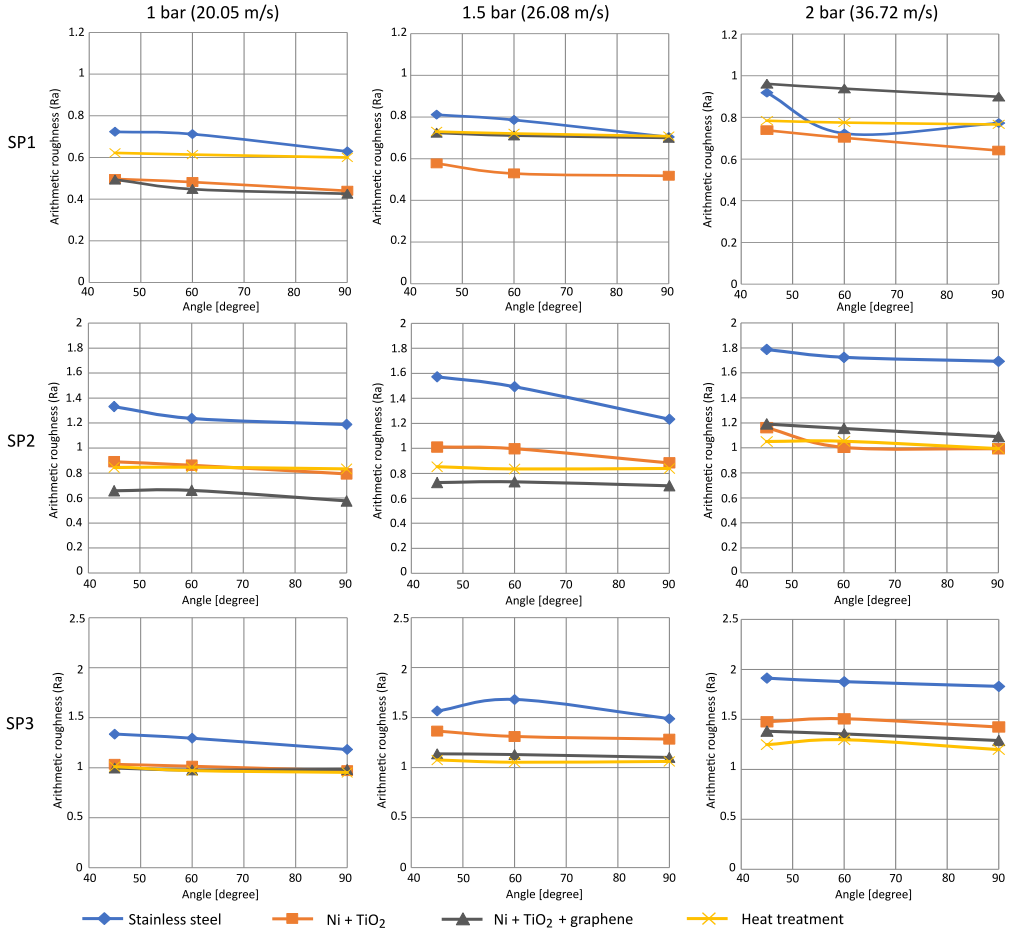

FIG. 7. Arithmetic roughness (μm) at different SP, impact angles (degrees) and impact speeds.

close to these of the heat-treated specimens. For SP1, Ni-TiO_2-coated specimens display the lowest roughness for all pressures and angles when SP1 is used, while for SP2, it can be observed that Ni-TiO_2-graphen-coated specimens yield the lowest roughness almost for all pressures and angles. The main difference between the curves for SP3 in Fig. 7 and those for SP1 and SP2 is the distinct and consistent sequence of the roughness for the four types of specimens. These curves indicate that for SP3, the lowest roughness is found in heat-treated specimens, followed very closely by Ni-TiO_2-graphene specimens, then the Ni-TiO_2 specimens, and finally stainless steel with the highest roughness. Figure 8 shows the surfaces before and after the tests for one testing condition at 2 bar, 45° and using SP3, while the SEM images in Fig. 9 illustrate the surfaces before and after the tests at different testing conditions.

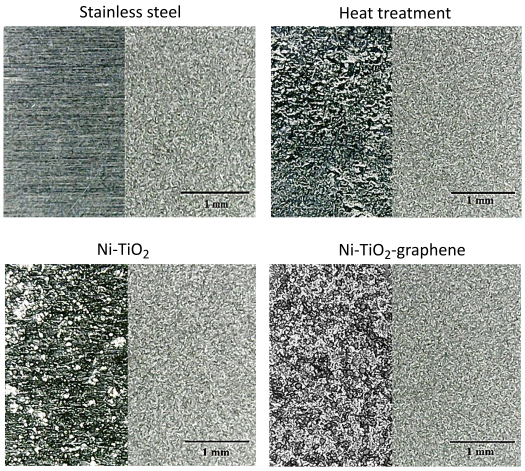

FIG. 8. Illustration of the surfaces before (left) and after test (right) at 2 bar, 45° and using SP3.

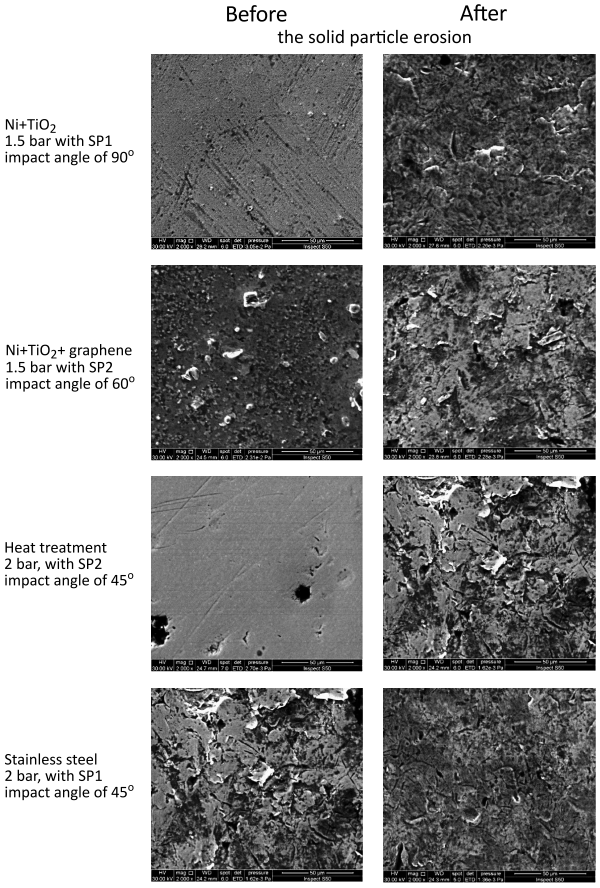

FIG. 9. SEM for the samples before and after the solid particle erosion.

5.2.2. Arithmetic roughness (Ra) in two directions. Optical and scanning electron microscopic images show waviness in the direction of blasting, as shown in Fig. 10. Therefore, the effect of erosion direction on surface roughness is investigated at various angles and a jet pressure of 2 bar, as surface modification becomes more apparent under high pressure. Figure 11 illustrates the results of the arithmetic roughness for different types of SP with various impact angles and under a pressure of 2 bar for all the samples. Roughness measurements were carried out in two directions: one in the up-down direction (the direction of the jet) and the other in left-right direction (normal to the jet direction). It is evident from this figure that there is a significant difference, almost double, in roughness between the two t directions when the angle is 45°and the solid particles SP1, microspherical particles, are used. This effect of SP1 at this angle is observed in all four types of specimens. For SP2 and SP3, the difference is less pronounced than that for SP1 and the Ni-TiO_2 coating shows almost the same roughness value in both directions.

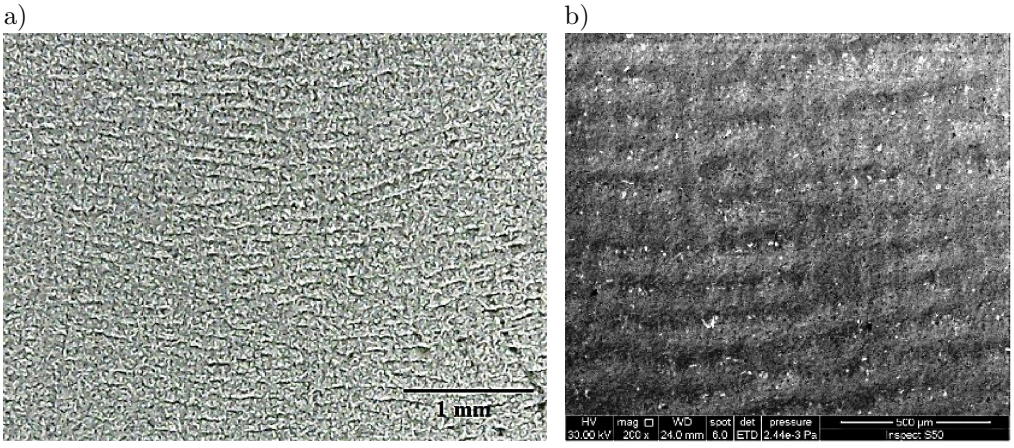

FIG. 10. Illustration of the waviness observed when SP1 is used and an impact angle is at 45°: a) optical microscopic image for the Ni-TiO_2 coating impacted with SP1 at 1.5 bar and 45°, b) SEM image for 410 stainless steel impacted with SP1 at 2 bar and 45°.

The variation in roughness in both directions indicates that at this angle, there is plastic deformation and/or plowing in the direction of impact, which generate a wavy pattern on the surface. However, it seems that only SP1 causes significant waviness, which may be due to the small size of particles resulting in indents with higher stress and strain, as the non-conformal contact area is small compared to the larger spherical solid particles of SP2, where the contact area is larger, resulting in reduced stress and strain. Another justification could be the higher kinetic energy of the larger particles that may cause direct material removal, while the lower kinetic energy of the smaller particles may result in

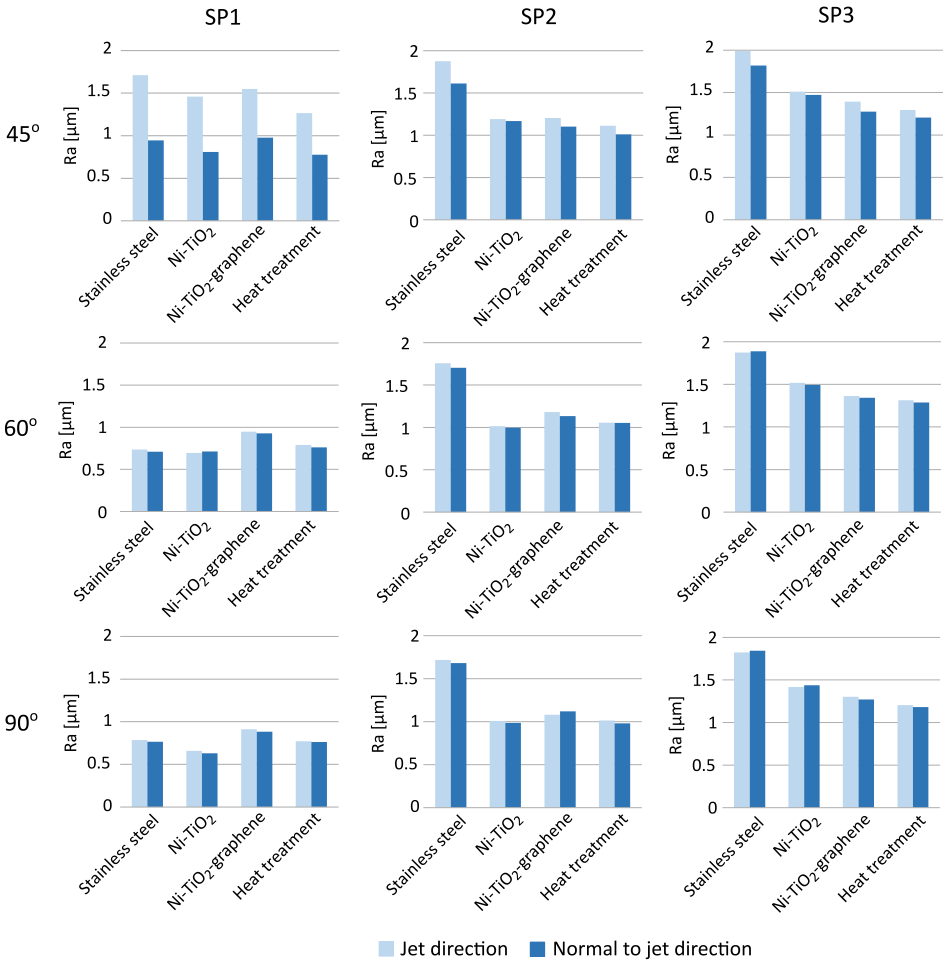

FIG. 11. The arithmetic roughness measured in the jet direction and normal to it under a pressure of 2 bar.

gradual and accumulated indentations that lead to plastic flow at shallow depth to form the waviness. On the other hand, SP3 leads to more cutting without considerable plastic flow to result in corrugation, similar to that caused by curved surfaces.

To investigate the occurrence of waviness in different directions, the roughness in both directions are measured for impact angles of 60° and 90°. It can be seen that the roughness is nearly identical in both directions for all types of specimens and when using all three types of solid particles. This shows that insufficient tangential force is generated at these angles to cause waviness deformation. Waviness deformation only seems to occur at 45° for the investigated solid particles and at 2 bars.

6. Calculation of wear coefficient and wear rate

Equations (4.1)–(4.5) were used to calculate the wear coefficient, wear rate constants and wear rate for each case, as shown in Table 6 and Fig. 12.

Table 6. Wear coefficient and wear rate constants.

Material	Sand type	$\alpha = 90°$			$\alpha = 60°$			$\alpha = 45°$		
		K	n	B	K	n	B	K	n	B
Stainless steel	1	0.104	0.563	0.767	0.041	0.930	0.303	0.035	1.029	0.259
	2	0.307	0.384	2.265	0.628	0.264	4.621	0.296	0.604	2.183
	3	0.337	0.606	2.489	0.440	0.562	3.239	1.442	0.301	10.573
Heat treatment	1	0.035	0.779	0.176	0.014	1.217	0.078	0.017	1.180	0.097
	2	0.100	0.620	0.544	0.664	0.136	3.601	1.199	0.102	6.450
	3	0.514	0.299	2.784	0.750	0.280	4.066	0.752	0.353	4.076
Ni/TiO_2	1	0.004	1.607	0.015	0.002	1.849	0.008	0.385	0.512	1.558
	2	0.125	0.800	0.507	0.185	0.835	0.749	0.430	0.654	1.741
	3	0.632	0.486	2.555	0.213	0.871	0.863	0.179	0.928	0.723
Ni-TiO_2-graphene	1	0.153	0.610	0.940	0.06	0.950	0.369	0.137	0.776	0.845
	2	0.708	0.250	4.357	0.099	0.892	0.609	0.355	0.591	2.189
	3	0.418	0.514	2.573	0.131	0.888	0.810	0.411	0.544	2.530

Figure 12 shows the wear rate, considering weight loss and the number of solid particles impacting the surface. It can be seen that the highest wear rate occurs at an impact angle of 45°for all specimens and under the impact of various solid particles. Also, the greatest wear rate is caused by SP3, followed by SP2, and SP1 with the least wear rate under all investigated impact angles and speeds.

As discussed in Subsec. 2.4, the hardness of SP3 could be slightly higher than that of SP1 and SP2. However, this may not be the cause for the higher wear rate caused by SP3. On the contrary, the distinct sharp edges of SP3, compared to the other particles used in this study, can be the main cause for the significant difference in the wear rate caused by this erodent. The percentage of wear rate enhancement can be calculated by comparing the wear rate to that of the stainless steel samples, as shown in Fig. 13. It is observed that the heat-treated specimens show the least wear rate almost for all tests with enhancement rate of 53.75% when SP3, a 45° impact angle and a speed of 36.72 m/s are used.

Under similar conditions, the Ni-TiO_2-graphene can be considered as the second best after the heat-treated specimens, with an enhancement rate of 36%, while an enhancement rate for the Ni-TiO_2 coating is 35.2%. A relatively higher percentage of improvement occurs at an impact angle of 90° for the heat-treated specimens with an improvement of 59.6%, while the Ni-TiO_2 and the Ni-TiO_2-graphene show a relatively lower improvement rates of 25.8%

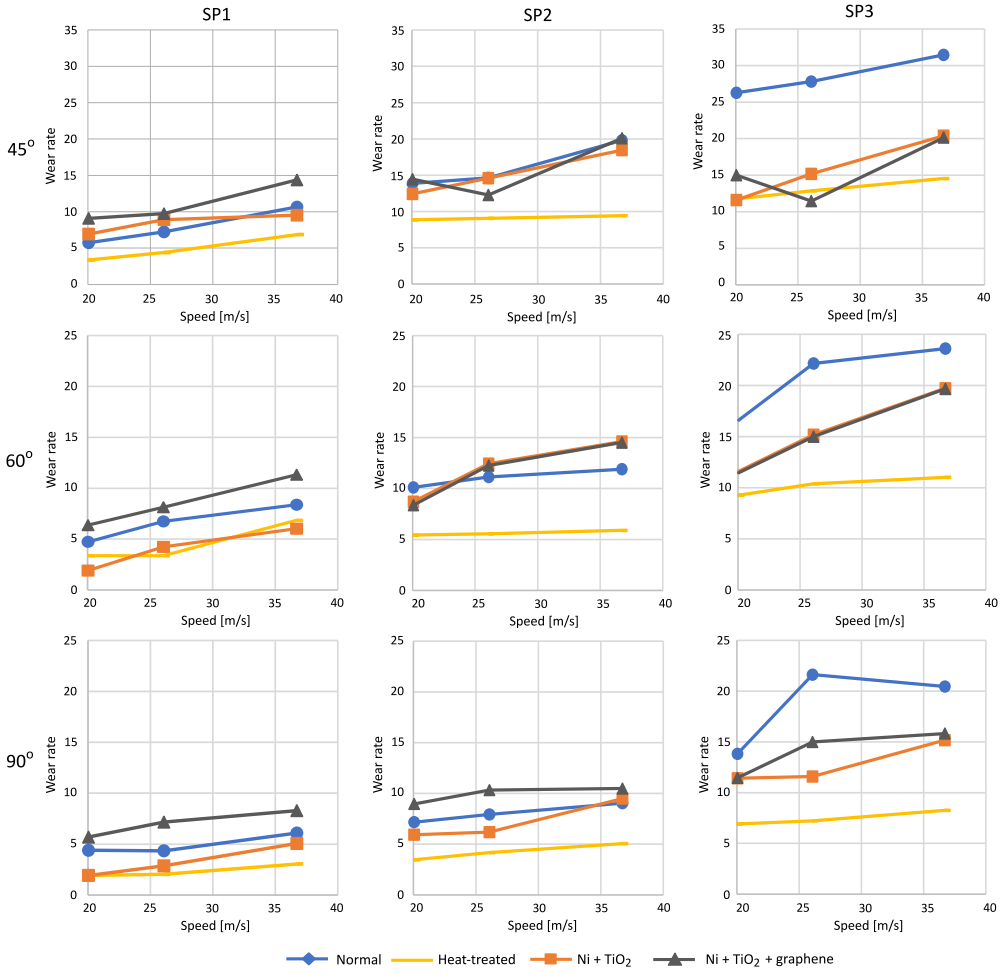

FIG. 12. Wear rate [mg/kg] at different SP, impact angles and impact speeds.

and 22.6%, respectively. In order to show the effectivity of the anti-wear techniques investigated in the current study, a comparison for the percentage of improvement with Diamond-Like Carbon (DLC) coating is shown in Fig. 13, where the extreme conditions when using SP3 impacting at 45° are considered. A recent study [25], showed that the DLC coating, which is one of the hardest protective coatings [26], can be highly effective against SPE. Figure 13 shows that heat treatment may results in almost the same level of protection as the DLC coating. However, the complexity of producing the DLC coating through the Plasma Enhanced Chemical Vapor Deposition (PECVD) encourages the use of simpler techniques, such as heat treatment and electroplating adopted in the current study, to achieve considerable resistance against SPE. This makes them significantly important in this context. The coatings, even if they show a lower

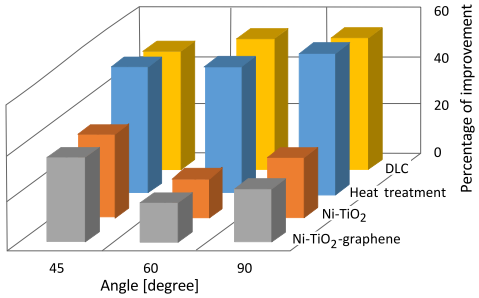

FIG. 13. Percentage of wear rate enhancement at an impact speed of 36.72 m/s and using SP3. The enhancement by DLC is added for comparison [25].

percentage of improvement, are still quite effective when considered as sacrificing layers that limit substrate weight loss, as discussed in Subsec. 5.1. In addition, using these coating reduces the surface roughness after SPE, as discussed in Subsec. 5.2.

Despite showing the highest improvement percentage for the heat treated steel, this study reveals the highest variation in wear rate when the impact angle is changed. For instance, under the highest impact speed and using SP1, the increase in wear rate when the angle changes from 90° to 45° is 73.4% for Ni-TiO_2-graphene, while it is 125% for the heat-treated steel. The same applies to SP3, where the increase in wear rate when the angle changes from 90° to 45° is 27.3% for Ni-TiO_2-graphene while it is 76.2% for the heat-treated steel with the highest impact speed and SP3 used.

By comparing the results in Fig. 12 with the values of K in Table 6, it can be seen that the lowest wear rate is not always associated with the lowest value of K without considering the value of n. The curves in Fig. 12 also show increase of wear rate with increasing the particles speeds. However, the slope of these curves varies from case to case, with some curves showing a strong dependency on speed (steep curves) and other curves exhibiting a slight dependency on speed (almost horizontal curves). This can be seen from the values of n in Table 6.

Overall, this study provides the required parameters to estimate the wear rate of the specimens investigated in the current study. This wear rate can be estimated for cases with different impact angles and speeds.

7. Conclusions

In the current study, the resistance of stainless steel 410 to SPE that are mainly SiO_2 was investigated. The effect of heat treatment, Ni-TiO_2 and Ni-TiO_2-graphene coatings on the wear rate and surface roughness was studied. Three types of solid particles, three impact angles and three impact speed were considered.

The following are the main conclusions based on the findings of this study:

1) Ni-based coatings are widely used in different applications. In the current study, adding nano TiO_2 to increase the hardness was found to be effective against SPE and surface roughness variation. Additionally, The effect of adding solid lubrication properties on SPE was investigated with the incorporation of graphene. The Ni-TiO_2-graphene considerably reduced surface roughness variation and improved the wear rate in specific cases, particularly at high jet pressures (1.5 or 2 bar) and using sharp particles (SP3).
2) The wear rate enhancement percentages reached 35.2% for the sample coated with Ni-TiO_2, 36% for the sample coated with Ni-TiO_2-graphene, and 53.75% for the heat-treated sample when using SP3, a 45° impact angle and a speed of 36.72 m/s. Accordingly, the investigated coatings and the heat treatment were beneficial in reducing wear.
3) Higher impact angle resulted in lower wear rates, which revealed a ductile erosion mechanism. It was observed that the increase in the wear rate occurred when the impact angle changed from 90° to 45°. For example, for the heat-treated steel, it may reach 125% while it is only 73.4% for Ni-TiO_2-graphene. It can be concluded that the wear resistance can vary significantly under different impact angles and improving the surface plays an important role in reaching a more stable performance under different impact angles, which was presented in this study using the investigated coatings.
4) Surface roughness after SPE may be important in many applications. It can be concluded that surfaces showing lower wear rate may not necessarily show less change in surface roughness. Metal composite coatings were found to be beneficial in reducing the surface roughness after SPE.
5) Although bigger particles and sharper particle geometry cause more deterioration to the surface, the current study revealed that smaller particles with a smooth surface can cause higher roughness in the form of waviness when the roughness is measured in a direction normal to the jet direction, especially when the impact occurs at 45°. It can be concluded that in certain conditions, surface deformation can be more significant than other wear mechanisms, such as cutting and plowing.
6) This study provides wear rate calculation parameters: K, B and n for Ni-TiO_2 and Ni-TiO_2-graphene coatings on 410 stainless steels substrate, as well as heat treated 410 stainless steels without coating, under various solid particle speeds, impact angles and types of eroding particles. These valuable parameters allow the estimation of wear rates for the investigated materials under different conditions.

References

1. Immarigeon J.P., Chow D., Parameswaran V.R., Au P., Saari H., Koul A.K., Erosion testing of coatings for aero engine compressor components, *Advanced Performance Materials*, **4**(4): 371–388, 1997, doi: 10.1023/A:1008644527599.
2. Alqallaf J., Ali N., Teixeira J.A., Addali A., Solid particle erosion behaviour and protective coatings for gas turbine compressor blades – A review, *Processes*, **8**(8): 984, 2020, doi: 10.3390/PR8080984.
3. Sharma V., Kaur M., Bhandari S., Singh S., Influence of velocity, concentration, and size of silt particles on erosion of thermal sprayed $Ni/TiO_2/Al_2O_3$ coatings, *Surface Review and Letters*, **2240001**, 2022, doi: 10.1142/S0218625X22400017.
4. Bousser E., Martinu L., Klemberg-Sapieha J.E., Solid particle erosion mechanisms of protective coatings for aerospace applications, *Surface and Coatings Technology*, **257**: 165–181, 2014, doi: 10.1016/j.surfcoat.2014.08.037.
5. Finnie I., Erosion of surfaces by solid particles, *Wear*, **3** (2): 87–103, 1960, doi: 10.1016/0043-1648(60)90055-7.
6. Hutchings I., Shipway P., *Tribology Friction and Wear of Engineering Materials*, 2nd ed., Butterworth-Heinemann, 2017, doi: 10.1016/B978-0-08-100910-9.09988-8.
7. Tilly G.P., A two stage mechanism of ductile erosion, *Wear*, **23**(1): 87–96, 1973, doi: 10.1016/0043-1648(73)90044-6.
8. Bellman Jr. R., Levy A., Erosion mechanism in ductile metals, *Wear*, **70**(1): 1–27, 1981, doi: 10.1016/0043-1648(81)90268-4.
9. Hassani S., Bielawski M., Beres W., Martinu L., Balazinski M., Klemberg-Sapieha J.E., Predictive tools for the design of erosion resistant coatings, *Surface and Coatings Technology*, **203**(3–4): 204–210, 2008, doi: 10.1016/j.surfcoat.2008.08.050.
10. Azzi M., Amirault P., Paquette M., Klemberg-Sapieha J.E., Martinu L., Corrosion performance and mechanical stability of 316L/DLC coating system: Role of interlayers, *Surface and Coatings Technology*, **204**(24): 3986–3994, 2010, doi: 10.1016/j.surfcoat.2010.05.004.
11. Zeng X.T., Goto T., Zhao L.R., Ding X.Z., Liew S.C., Li G.Y., Erosive wear properties of Ti-Si-N nanocomposite coatings studied by micro-sandblasting, *Journal of Vacuum Science & Technology A: Vacuum, Surfaces, and Films*, **23**(2): 288–292, 2005, doi: 10.1116/1.1861053.
12. Wei R., Rincon C., Langa E., Yang Q., Microstructure and tribological performance of nanocomposite Ti-Si-C-N coatings deposited using hexamethyldisilazane precursor, *Journal of Vacuum Science & Technology A: Vacuum, Surfaces, and Films*, **28**(5): 1126–1132, 2010, doi: 10.1116/1.3463709.
13. Bousser E., Martinu L., Klemberg-Sapieha J.E., Solid particle erosion mechanisms of hard protective coatings, *Surface and Coatings Technology*, **235**: 383–393, 2013, doi: 10.1016/j.surfcoat.2013.07.050.
14. Bousser E., Benkahoul M., Martinu L., Klemberg-Sapieha J.E., Effect of microstructure on the erosion resistance of Cr-Si-N coatings, *Surface and Coatings Technology*, **203**(5–7): 776–780, 2008, doi: 10.1016/j.surfcoat.2008.08.012.
15. Shao W., Nabb D., Renevier N., Sherrington I., Luo J.K., Mechanical and corrosion resistance properties of TiO_2 nanoparticles reinforced Ni coating by electrodeposition, *IOP Conference Series: Materials Science and Engineering*, **40**(1): 1–6, 2012, doi: 10.1088/1757-899X/40/1/012043.

16. Uysal M., Algül H., Duru E., Kahraman Y., Alp A., Akbulut H., Tribological properties of Ni-W-TiO_2-GO composites produced by ultrasonically-assisted pulse electro co-deposition, *Surface and Coatings Technology*, **410**: 126942, 2021, doi: 10.1016/j.surfcoat.2021.126942.

17. De Lima M.S.F., Do Espirito Santo A.M., Phase transformations in an AISI 410S stainless steel observed in directional and laser-induced cooling regimes, *Materials Research*, **15**(1): 32–40, 2012, doi: 10.1590/S1516-14392012005000003.

18. Chen W., He Y., Gao W., Electrodeposition of sol-enhanced nanostructured Ni-TiO_2 composite coatings, *Surface and Coatings Technology*, **204**(15): 2487–2492, 2010, doi: 10.1016/j.surfcoat.2010.01.036.

19. Yasin G., Arif M., Nizam M.N., Shakeel M., Khan M.A., Khan W.Q., Hassan T.M., Abbas Z., Farahbakhsh I., Zuo Y., Effect of surfactant concentration in electrolyte on the fabrication and properties of nickel-graphene nanocomposite coating synthesized by electrochemical co-deposition, *RSC Advances*, **8**(36): 20039–20047, 2018, doi: 10.1039/c7ra13651j.

20. Bukowski B., Deskins N.A., The interactions between TiO_2 and graphene with surface inhomogeneity determined using density functional theory, *Physical Chemistry Chemical Physics*, **17**(44): 29734–29746, 2015, doi: 10.1039/c5cp04073f.

21. American Society for Metals, *Atlas of Microstructures of Industrial Alloys*, Taylor Lyman [Ed], 8th ed., ASM, Metals Park, Ohio, 1972.

22. Reade International Corp, Mohs' Hardness (Typical) of Abrasives, *Reade International Corp*, 2020, https://www.reade.com/reade-resources/reference-educational/reade-reference-chart-particle-property-briefings/mohs-hardness-typical-of-abrasives#:~:text=Most abrasives that effectively achieve,hardness of at least 6.0.&text=The Mohs' scale of hardness,a m (accessed Dec. 23, 2021).

23. American Society for Testing and Materials, G76-07, Standard Test Method for Conducting Erosion Tests by Solid Particle Impingement Using Gas Jets, *ASTM International*, **G76-18**: 1–6, 2018, doi: 10.1520/G0076-18.2.

24. Kleis I., Kulu P., *Solid Particle Erosion: Occurrence, Prediction and Control*, Springer-Verlag, London, 2008, doi: 10.1007/978-1-84800-029-2.

25. Al-Asadi M.M., Al-Tameemi H.A., The effect of diamond like carbon coating on the solid particles erosion resistance of grade 410 stainless steel, *Wear*, **514–515**: 204584, 2023, doi: 10.1016/j.wear.2022.204584.

26. Al-Asadi M.M., Al-Tameemi H.A., A review of tribological properties and deposition methods for selected hard protective coatings, *Tribology International*, **176**: 107919 2022, doi: 10.1016/j.triboint.2022.107919.

Received May 26, 2023; accepted version August 21, 2023.